TWO-DIMENSIONAL REPRESENTATION OF THE BIDIRECTIONAL REFLECTANCE DISTRIBUTION FUNCTION OF PHOTOVOLTAIC MODULES

Christof Bucher[1], Andreas Bohren[2], Donat Hess[1], Sara El Hassani[1], Matthias Hügi[1]

[1]Bern University of Applied Sciences (BFH), Switzerland; [2]Ostschweizer Fachhochschule (OST)

christof.bucher@bfh.ch, andreas.bohren@ost.ch, donat.hess@bfh.ch, sara.elhassani@bfh.ch, matthias.huegi@bfh.ch

The optical reflectance properties of PV modules can be described using the bidirectional reflectance distribution function (BRDF). In this paper, a simplified two-dimensional approach to represent the BRDF is proposed. The shape of the solar reflectance image on the PV module is described by comparing a mathematical model and two measurement approaches. For standard PV modules using anti-reflective solar glass, the shape of the solar reflection image is regular and typically elliptical and depends on the angle of solar incidence α. The elliptical shape is described using a diagram for each horizontal and vertical axis based on the constant luminance zone. The dimensions of the axes are approximated using an empirical mathematical function. The result can be used to include glare information in the data sheet of a PV module and to correctly implement the phenomenon of beam spread in tools for glare hazard analysis.

1 INTRODUCTION

Glare hazards on PV modules are an increasing concern in the build-over area, especially when eastern, western and northern roofs in the northern hemisphere are covered with PV modules [1], [2]. Glare analysis tools such as Sandias Solar Glare Hazard Analysis Tool (SGHAT, [3], [4]) typically model the beam spread as a symmetric phenomenon that is independent of the angle of incidence α. This leads to overestimation or underestimation of the effective glare duration. The correct modelling of the shape of the reflection beam is seen to be complex, because the structure of the glass surface is irregular and leads to irregular reflection cones[5], [6].

Although PV modules are typically coated with an anti reflective coating (ARC) and/or manufactured using a textured surface to maximise the light transmission through the solar glass they don't provide reliable protection against glare hazards[7].

Due to geometrical reasons tilted PV modules facing south in the northern hemisphere do normally not cause any glare hazards to the neighbouring area. However, due to cost reduction of photovoltaics, more and more rooftops are equipped with PV independent of the roof orientation. Thereby it was found that rooftops facing north are critical regarding glare hazards for observation points north of the building.

The most relevant factor to quantify glare is the luminance in cd/m^2, describing the "brightness" of a surface. Because the disturbance caused by glare depends on a large number of factors, no guideline or limit values have been published yet. Depending on the source, so-called absolute glare (saturation of the eyes) occurs from about 100,000 cd/m^2. However, disturbing effects that lead to an afterimage can already occur at significantly lower values [7], see also the next section "definition of glare".

Originally, glare reports were prepared for PV systems at airports. However, at least in Switzerland, more and more glare reports are being requested to clarify glare in neighbourhood disputes. Glare reports typically calculate at what time of day and year the physical law of reflection "angle of incidence = angle of emergence" is observed.

The beam spreading is either neglected or represented with a highly simplified procedure. The free tool for calculating glare in Switzerland (www.blendtool.ch [8]) as well as the SGHAT, for example, add the angle of beam spreading as a constant and angle-independent number to the reflection diagram. This is critical for two reasons:

1. The angle of beam spreading is not defined and not known for most glasses.
2. The beam spread is not constant but dependent on the angle of incidence α.

Information on reflections is sometimes reproduced on data sheets of PV modules. This information refers either to the angle-dependent reflection coefficient (Figure 1) or to the maximum expected angle-dependent luminance (Figure 2). While the reflection coefficient cannot be used to draw conclusions about the glare properties because it does not take beam spreading into account, the luminance provides the most important information about glare. However, luminance can only be used to determine how bright a PV module can be from which angle. The information on how large this bright spot is is missing, and it is therefore not possible to determine how long a glare can last. However, because the duration of glare is one of the main factors for assessing glare, the current data sheets of glare-reduced PV modules are only suitable for assessing possible glare to a limited extent.
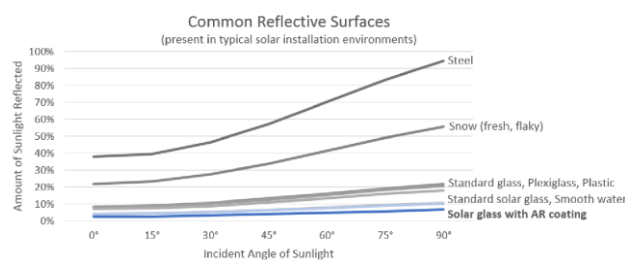

Figure 1: Amount of sunlight reflected as an indicator that solar glass has limited reflections only. This is mainly relevant to indicate high efficiency of PV modules, but does hardly affect glare. Data and graphics from Sunpower [9].
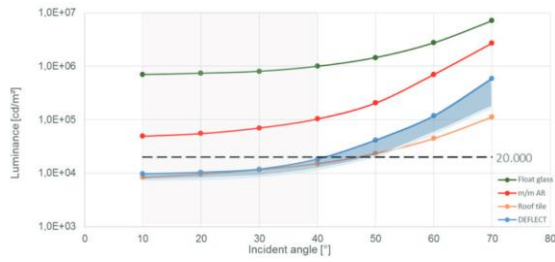
Figure 2: Glare representation of a PV module equipped with glare-reduced Deflect ® glass. Source: Data sheet [10].

2 DEFINITIONS

2.1. Definition of Glare

Depending on the situation different definitions of glare are found. The European standard EN 12665 "Light and lighting Basic concepts and criteria for specifying lighting requirements" [11] defines glare as an "unpleasant visual condition caused by unfavourable luminance distribution or excessive contrast". This very general definition touches on a wide range of different phenomena. Specifically, a disturbance that is subjectively perceived as unpleasant is called psychological glare ("discomfort glare"). Physiological glare or absolute glare, on the other hand, is a measurable impairment of the visual functions that can also lead to permanent damage to the retina.

Absolute glare is the situation in which the eye can no longer adapt to the brightness. Depending on the area of the light source and the aperture, luminance levels of $1.0 \cdot 10^4$ to $1.6 \cdot 10^5$ cd/m^2 lead to absolute glare [12]. With absolute glare, the eye can no longer adapt and above this limit, differences in brightness can no longer be perceived. From a medical point of view, it is advisable to avoid long-lasting situations with absolute glare. However, many common materials such as white plaster, glass or wet surfaces easily cause absolute glare in full sunlight. This means that absolute glare sensations are common in a normal environment.

Psychological glare (discomfort glare) is considered to induce a significant impairment of general well-being, work performance, safety, ability for concentration, etc. However, depending on the person and the situation, it is possible that even absolute glare does not necessarily lead to discomfort glare.

Different methods and standards have been developed to quantify glare. However, the best developed methods are for indoor use only and are applicable for the evaluation of illumination concepts.

In addition to luminance, there are various other quantities for determining glare. One of the best known is the "Unified Glare Rating" (UGR) developed by the "Commission International de l'Eclairage" (CIE). However, UGR was developed for small, point light sources in front of a dark background and is not suitable for evaluating the glare emitted by larger surfaces [13], [14].

However, in order to assess the glare on a PV module in reality, these definitions are only of limited use. In particular, these definitions do not take into account that virtually all surfaces can be glare under certain conditions, and yet are not considered to be glare. For this reason, this paper compared luminance measurements of different materials that are not associated with glare. A key factor in evaluating these materials is the angle of light incidence

α. For virtually any surface, the flatter the angle α, the greater the luminance of the surface. To evaluate whether a surface is perceived as glare or not, the measured materials are therefore compared with each other.

The maximum value of a material not associated with glare is proposed as the limit value for a PV module to be considered "glare-free" in this paper (Figure 3). This is angle-dependent and is only defined up to $\alpha = 80°$ (flat incidence angle). In reality, flatter angles α lead to double glare, i.e. the sunbeam and the glare beam come from practically the same direction. The glare beam is thus drowned out by the sun beam. Figure 3 shows the luminance levels of various surfaces measured by SPF. It also shows the resulting proposed limit value for assessing a PV module as a "glare-free PV module". The values for assessing the absence of glare are set at approx. 90% of the measured values in order to maintain a safety margin and are rounded generously for better usability.
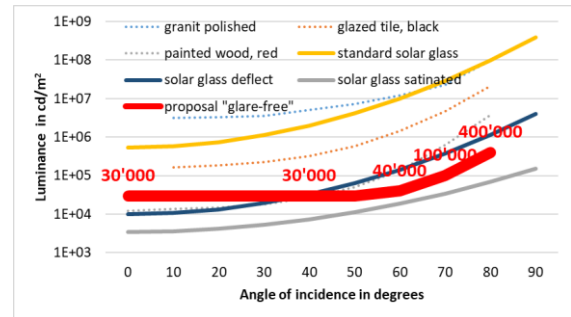

Figure 3: Luminance of different surfaces and proposed limit value for "glare-free PV modules".

2.2 Description of the Shape of Glare

From our daily experience, we know that glare on a PV module usually has an elliptical appearance (Figure 4). It is assumed, that the horizontal and vertical axis of this ellipse depend on the type of solar glass. The aim of this paper is to characterise and mathematically describe both the size and the shape of this elliptical appearance.

Figure 4: The appearance of glare is usually elliptical.

The exact size of the glare ellipse depends on the definition of the glare and the beam spread respectively. This is defined in the following section.

2.3. Definition of Beam Spread

Beam spread is a common concept for describing the shape of glare on a PV module. The following definition is used[3], [4], [17]:

$$\beta = 2 \cdot (4.65 + \sigma) \; mrad$$

Where $4.65 \; mrad$ is the subtended half-angle of the sun and σ is the slope error of the reflective surface. The factor of 2 accounts for the resulting reflected angle from the surface. As this equation assumes round (circular) reflection beams and does not depend on the incident

angle, it is not suitable for accurately model the shape of the glare.

Therefore, a new definition of beam spread is proposed in this paper. It is based on the assumption that the shape of glare is elliptic and consists of a horizontal and vertical axis. To calculate the horizontal and vertical axis of the reflection ellipse, two approaches are proposed.

- The contour line at 30'000 cd/m^2
- The Full With Half Maximum (FWHM) of the cone (see also Figure 12)

These two approaches are presented in the following sections.

Contour line at 30'000 cd/m^2

In this approach the glare ellipse is defined as the part of the image which exceeds 30'000 cd/m^2. In contrast to Figure 3, a constant threshold value is proposed in this paper. This is done to avoid arbitrary curves in the results. However, the threshold value is set to the value found for most angles in Figure 3, which is 30'000 cd/m². This corresponds approximately to the white areas in the pictures of Figure 4.

Full With Half Maxima (FWHM)

Instead of defining the area with a luminance larger than 30'000 cd/m^2 as the glare area, the glaring area can be described with the FWHM. However, this underestimates the size of the glare ellipse for standard solar glass and underestimates it for glasses with luminance values close to the glare limit.

3   METHODS TO DESCRIBE THE ELLIPSE

3.1 Geometrical model to calculate the horizontal and vertical axis of a glare ellipse

The approach of describing a glare as an ellipse is more phenomenological than scientific. The results are determined on the basis of calibrated measurements, not on the basis of a physical model. Nevertheless, a physical model is proposed in this chapter. This is intended to give the phenomenological observations a physical legitimation.

The physical model assumes that the glass surface is not flat but slightly modelled with high and low points. Accordingly, the areas between the high and low points do not lie in the supposed module plane, but at a certain flat angle to it. The modelling in this paper assumes that there are five surface areas on each surface element: One of them lies in the module plane, the other four are each inclined at constant angles in a cardinal direction. A glare ray is thus divided into five reflection rays (see Figure 5) neglecting the fact that in reality the surface does not have five discrete zones, but that these zones merge smoothly into one another. The five reflection rays symbolise the ends of the axes and the centre of the ellipse.
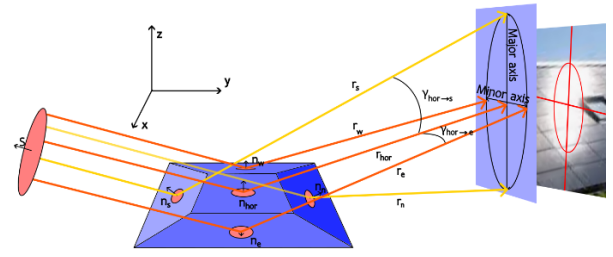

Figure 5: Geometrical approach to model the shape of the reflection

To calculate the reflection beams, the following definitions are made. For simplified representation, the module is placed in the plane of the coordinate system and the azimuth angle of the sun is defined as zero:

- Elevation angle of the sun: α
- Sun vector: $\vec{s} = \begin{pmatrix} 0 \\ cos\alpha \\ sin\alpha \end{pmatrix}$
- Angle difference between the plane of module and the maximum deviation: β
- Normal vector of the horizontal plane of module $\overrightarrow{n_{hor}} = \begin{pmatrix} 0 \\ 0 \\ 1 \end{pmatrix}$
- Normal vector of the east west deviated surface: $\overrightarrow{n_{ew}} = \begin{pmatrix} sin\beta \\ 0 \\ cos\beta \end{pmatrix}$
- Normal vector of the north south deviated surface: $\overrightarrow{n_{ns}} = \begin{pmatrix} 0 \\ sin\beta \\ cos\beta \end{pmatrix}$

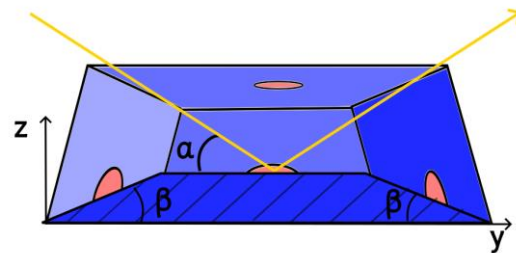The angles and vectors are shown in Figure 5 and Figure 6.

Figure 6: Definition of the angles used in this paper. The incidence angle α is used throughout the paper.

Based on the optical law "angle of incidence = angle of reflection", the reflection beam is calculated as $\vec{r} = \vec{s} - 2 \cdot (\vec{s} \cdot \vec{n}) \cdot \vec{n}$ for a normal vector $\vec{n}$ of the plane of reflection. For the three normal vectors $\overrightarrow{n_{hor}}$, $\overrightarrow{n_{ew}}$, and $\overrightarrow{n_{ns}}$ this results in the following reflection vectors $\overrightarrow{r_{hor}}$, $\overrightarrow{r_{ew}}$ and $\overrightarrow{r_{ns}}$:

$$\overrightarrow{r_{hor}} = \vec{s} - 2 \cdot \underbrace{(\vec{s} \cdot \overrightarrow{n_{hor}})}_{sin\alpha} \cdot \overrightarrow{n_{hor}} = \begin{pmatrix} 0 \\ cos\alpha \\ sin\alpha \end{pmatrix} - 2 \cdot sin\alpha \cdot \begin{pmatrix} 0 \\ 0 \\ 1 \end{pmatrix} = \begin{pmatrix} 0 \\ cos\alpha \\ -sin\alpha \end{pmatrix}$$

$$\overrightarrow{r_{ew}} = \vec{s} - 2 \cdot \underbrace{(\vec{s} \cdot \overrightarrow{n_{ew}})}_{sin\alpha \cdot cos\beta} \cdot \overrightarrow{n_{ew}}$$

$$= \begin{pmatrix} 0 \\ cos\alpha \\ sin\alpha \end{pmatrix} - 2 \cdot sin\alpha \cdot cos\beta \cdot \begin{pmatrix} sin\beta \\ 0 \\ cos\beta \end{pmatrix}$$

$$= \begin{pmatrix} -2 \cdot sin\alpha \cdot cos\beta \cdot sin\beta \\ cos\alpha \\ sin\alpha - 2 \cdot sin\alpha \cdot cos\beta \cdot cos\beta \end{pmatrix}$$

$$\overrightarrow{r_{ns}} = \vec{s} - 2 \cdot \underbrace{(\vec{s} \cdot \overrightarrow{n_{ns}})}_{\substack{cos\alpha \cdot sin\beta + sin\alpha \cdot cos\beta \\ = sin(\alpha+\beta)}} \cdot \overrightarrow{n_{ns}}$$

$$= \begin{pmatrix} 0 \\ cos\alpha \\ sin\alpha \end{pmatrix} - 2 \cdot sin(\alpha + \beta) \cdot \begin{pmatrix} 0 \\ sin\beta \\ cos\beta \end{pmatrix}$$

$$= \begin{pmatrix} 0 \\ cos\alpha - 2 \cdot sin(\alpha + \beta) \cdot sin\beta \\ sin\alpha - 2 \cdot sin(\alpha + \beta) \cdot cos\beta \end{pmatrix}$$

However, it is not the reflection vectors themselves that are of interest, but the angles $\gamma_{hor\rightarrow ew}$ and $\gamma_{hor\rightarrow ns}$ between the reflection vector at the module plane and the other reflection vectors. Because all vectors are normalised in length, the angle between two vectors is calculated with the help of the scalar product as follows:

$$cos\gamma_{hor\rightarrow ew}(\alpha, \beta) = \frac{\overrightarrow{r_{hor}} \cdot \overrightarrow{r_{ew}}}{\underbrace{|\overrightarrow{r_{hor}}|}_{1} \cdot \underbrace{|\overrightarrow{r_{ew}}|}_{1}} = \overrightarrow{r_{hor}} \cdot \overrightarrow{r_{ew}}$$

$$= \begin{pmatrix} 0 \\ cos\alpha \\ -sin\alpha \end{pmatrix} \cdot \begin{pmatrix} -2 \cdot sin\alpha \cdot cos\beta \cdot sin\beta \\ cos\alpha \\ sin\alpha - 2 \cdot sin\alpha \cdot cos\beta \cdot cos\beta \end{pmatrix}$$
$$= (cos\alpha)^2 - (sin\alpha)^2 + 2 \cdot (sin\alpha)^2 \cdot (cos\beta)^2$$

$$cos\gamma_{hor\rightarrow ns}(\alpha, \beta) = \frac{\overrightarrow{r_{hor}} \cdot \overrightarrow{r_{ns}}}{\underbrace{|\overrightarrow{r_{hor}}|}_{1} \cdot \underbrace{|\overrightarrow{r_{ns}}|}_{1}} = \overrightarrow{r_{hor}} \cdot \overrightarrow{r_{ns}}$$

$$= \begin{pmatrix} 0 \\ cos\alpha \\ -sin\alpha \end{pmatrix} \cdot \begin{pmatrix} 0 \\ cos\alpha - 2 \cdot sin(\alpha + \beta) \cdot sin\beta \\ sin\alpha - 2 \cdot sin(\alpha + \beta) \cdot cos\beta \end{pmatrix}$$
$$= (cos\alpha)^2 - 2 \cdot cos\alpha \cdot sin(\alpha + \beta) \cdot sin\beta - (sin\alpha)^2 + 2 \cdot sin\alpha \cdot sin(\alpha + \beta) \cdot cos\beta$$
$$= cos(2\beta)$$

The last two equations thus give the horizontal and vertical axes of the presumed reflection ellipse. Figure 7 shows the two angles graphically. With this representation alone, the elliptical shape can be justified, but not the observed increase in the major axis of the ellipse at flat angles.

The angle of the minor axis is defined by $\gamma_{hor\rightarrow ew}(\alpha)$. Like the angle of the major axis, it starts at $\gamma_{hor\rightarrow ew}(0°) = 2\beta$ for $\alpha = 0°$ (perpendicular to the module surface), but converges towards $\gamma_{hor\rightarrow ew}(90°) = 0°$ for $\alpha = 90°$. The angle of the main axis, on the other hand, is independent of α and is $\gamma_{hor\rightarrow ns}(\alpha) = 2\beta$ for all incident angles. This consideration only applies for $\alpha \geq \beta$ (Figure 5)
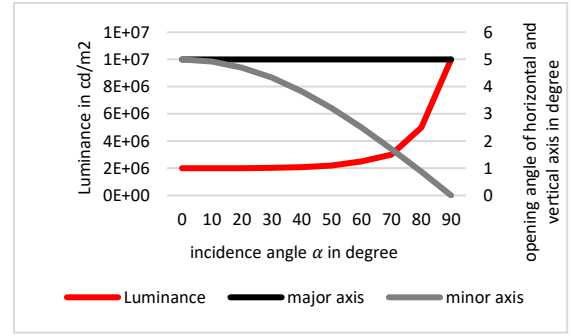

Figure 7: Numeric result of horizontal and vertical axis for the angle $\beta = 1.25°$

Figure 7 suggests that an ellipse can be observed. However, this ellipse would become smaller and smaller as the angle α increases. This does not correspond to the observations. In order to describe the phenomenon of the ellipse becoming larger, the model from Figure 5 must be modified.

Figure 5 assumes that the horizontal and vertical axes of the ellipse are given by a clearly defined angle, caused by the discretely divided surface structure. In reality, however, the five discrete zones merge smoothly into one another and therefore the ellipse does not have clear dimensions but becomes faded with increasing distance from the centre. The photographed ellipse results from the saturation of the camera sensor. At the same settings, the sensor saturates at the same luminance each time. Because the luminance of the blurred ellipse increases with increasing α, the glare limit shifts outwards.

To illustrate this observation, it is assumed in the following that the angle β increases proportionally to the logarithm of the luminance. The increase in β is argued by the fact that as α increases, reflections greater than 30'000 cd/m² are possible for surface areas with larger southward tilt β. The proportionality factor is not known and is arbitrarily set at 1. Thus, if the luminance increases by a factor of 10 (i.e. by 1 power of ten), β increases by a factor of 1. Figure 9 shows the resulting axis sizes.
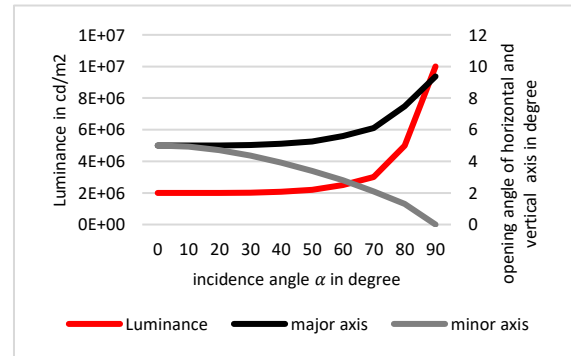

Figure 8: Modification of Figure 7: Opening angle of horizontal and vertical axis, corrected by the Luminance.

The reduction of the minor axis size with increasing α does not agree with all observations. This can be explained by the fact that our model only considers planes with north/south and east/west orientation. Such planes cannot deflect irradiation with large α laterally. A diagonal surface with, for example, south/west or south/east orientation could. In order to make the model more

accurate, such planes would therefore also have to be taken into account.

With this model, the observed phenomena can be explained partially, but not completely. In the following of this paper, we will therefore not work with the geometric model, but with the metrological investigations.

3.2. Phenomenological approach to the representation of the ellipse

In this approach, the glare on a standard photovoltaic module is photographed at different observer distances, different orientations of the PV module and for a variation of observation angles. The camera is set so that the sensor goes into saturation at approx. 30'000 cd/m^2. Thus, the white areas in the photos are a appropriate visualisation of the glare.

In addition, the software iQ-Luminance from the company Image Engineering GmbH & Co. KG is used to convert the photos into luminance images. Since one camera setting only allows for reliable luminance values within a decade, each luminance image is based on six serial pictures, each with decreasing exposure times or increasing aperture values. The six luminance images were then merged into one image, considering only those areas of each image where the pixel sensors were neither oversaturated nor undersaturated. This allows to create a luminance picture of the hole glare.

Figure 9 serves as example of such a luminance image. The angles 1°, 5°, 10°, 20° are shown as concentric circles around the glare maximum to allow qualitative estimation of the glare size. The white contour line represents the iso line of 30'000 cd/m^2 and the red line its elliptical approximation. The good correspondence between the 30'000 cd/m^2 iso line and the elliptic fit confirms the assumption that the glare has an elliptic shape. Therefore, only the fit curve is shown in the subsequent plots. The horizontal and vertical axes of the fit allow the size of the glare to be quantified.
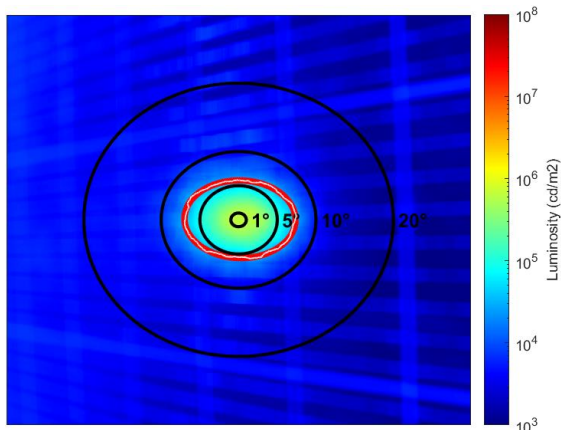

Figure 9: Luminance image of a glare, with the 30'000 cd/m^2 iso line (thin white) and its elliptic approximation (red). Concentric angles (1°, 5°, 10° and 20°) around the center of the glare are shown in black.

Photos of PV modules from different distances show that the size of the glare is independent of the distance of the observer for standard and float glasses (see Figure 10).

Figure 10: Phenomenological approach to show the independence of horizontal and vertical axis of the glare ellipse from the distance of the observer for standard (upper row) and float module (lower row)

Glare images of differently oriented modules (horizontal and vertical), under constant irradiation angle, show no difference in the case of the float glass but do show differences in the case of the standard glass module Figure 11. In this case, the difference in the length of the major axis is noticeable.
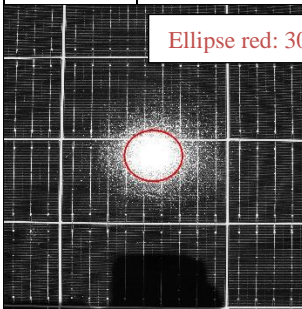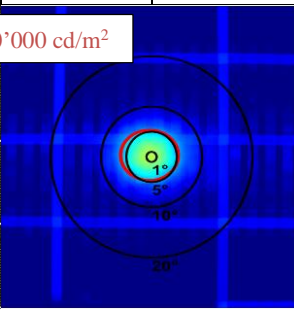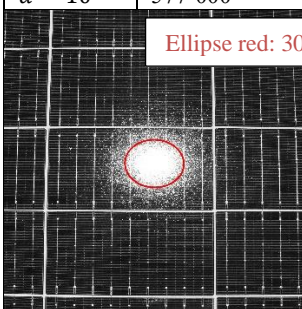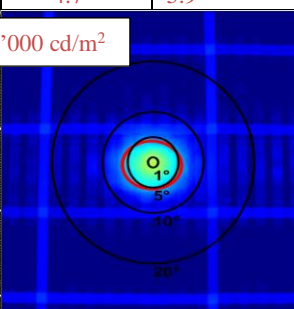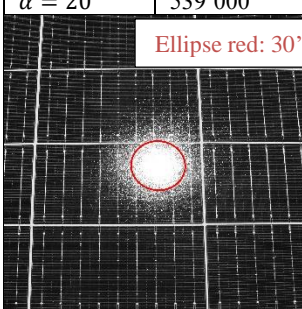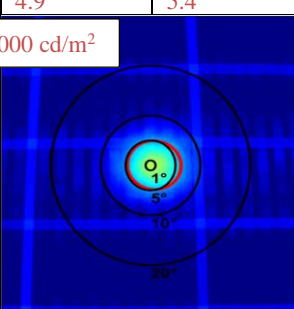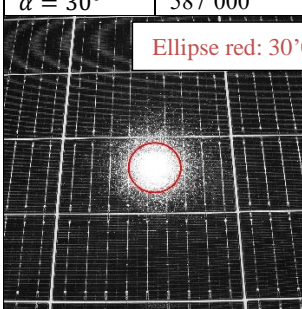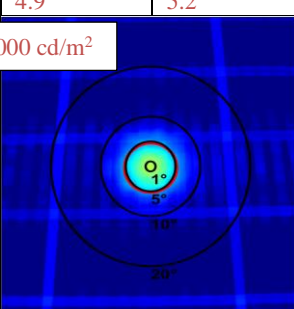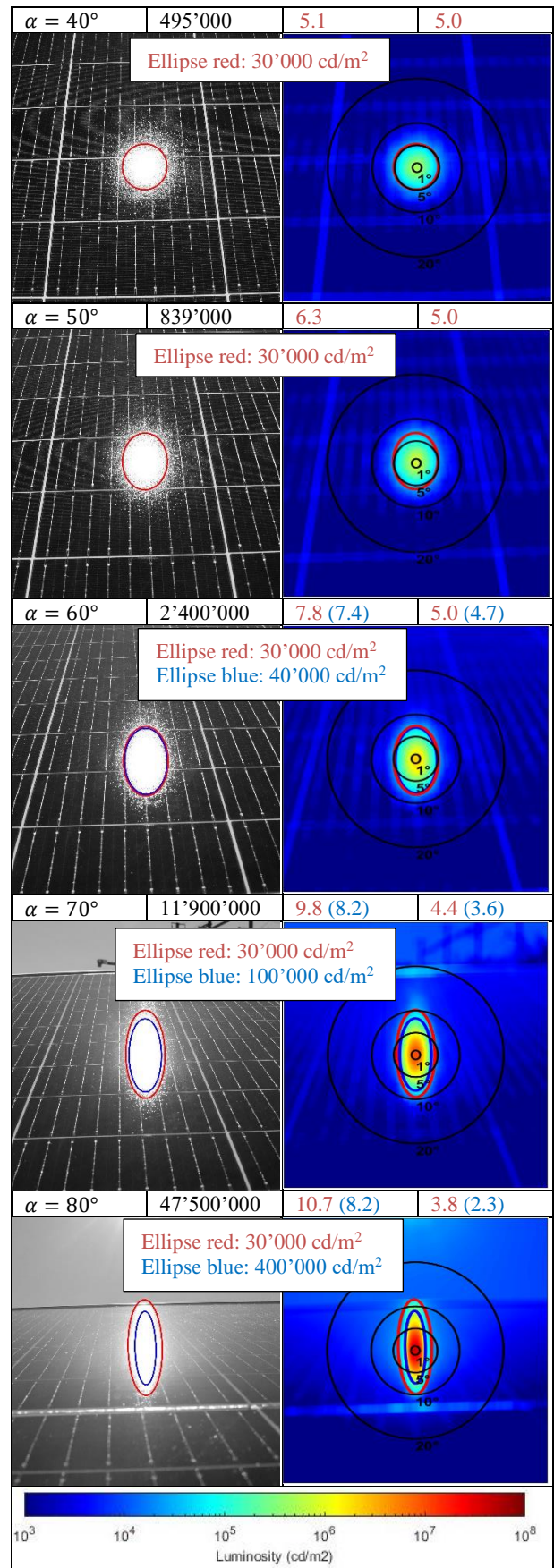

Figure 11: Phenomenological approach to investigate the influence of PV module orientation on the horizontal and vertical axes of the glare ellipse for standard (top row) and float (bottom row) modules.

To investigate the dependence of the glare of a standard module on α, photos (saturation at ca. 30'000 cd/m^2) and luminance images were generated for nine

different angles between 5° and 80°. Based on the luminance images, the maximum luminance as well as the horizontal and vertical length of the glare ellipse were determined (Table I).

Table I: Photographed glare and the corresponding luminance image for different α.

Optical picture		Luminance image	
α (°)	Luminance max cd/m²	Vertical axis (°)	Horizonal axis (°)
$\alpha = 5°$	594'000	5.0	5.7

Ellipse red: 30'000 cd/m²

| $\alpha = 10°$ | 577'000 | 4.7 | 5.9 |

Ellipse red: 30'000 cd/m²

| $\alpha = 20°$ | 539'000 | 4.9 | 5.4 |

Ellipse red: 30'000 cd/m²

| $\alpha = 30°$ | 587'000 | 4.9 | 5.2 |

Ellipse red: 30'000 cd/m²

| $\alpha = 40°$ | 495'000 | 5.1 | 5.0 |

Ellipse red: 30'000 cd/m²

| $\alpha = 50°$ | 839'000 | 6.3 | 5.0 |

Ellipse red: 30'000 cd/m²

| $\alpha = 60°$ | 2'400'000 | 7.8 (7.4) | 5.0 (4.7) |

Ellipse red: 30'000 cd/m²
Ellipse blue: 40'000 cd/m²

| $\alpha = 70°$ | 11'900'000 | 9.8 (8.2) | 4.4 (3.6) |

Ellipse red: 30'000 cd/m²
Ellipse blue: 100'000 cd/m²

| $\alpha = 80°$ | 47'500'000 | 10.7 (8.2) | 3.8 (2.3) |

Ellipse red: 30'000 cd/m²
Ellipse blue: 400'000 cd/m²

3.3 BRDF Approach

In a third, phenological approach using calibrated indoor laboratory measurements, the shape of the glare beam and thus the size of the horizontal and vertical axis are calculated using the bidirectional reflectance distribution function (BRDF). In a generic approach this can be done by approximating the BRDF conical shape with a two-dimensional Gaussian curve. As described in Chapter 2, both the FWHM and the contour line approach can be used to describe the elliptic shape of the cross section of the cone in Figure 12.

In contrast to the measurement method from Chapter 3.2, the BRDF measurement in the laboratory has the advantage that it is independent of the weather and can therefore be repeated at any time. The disadvantage, however, is that only a small area of the PV modules is measured. If there are inhomogeneities on the PV module, which can be caused, for example, by the conductor tracks in the modules, the BRDF measurement can no longer be used. During the measurement, it must be defined which point on the module is measured, which has a major influence on the result.
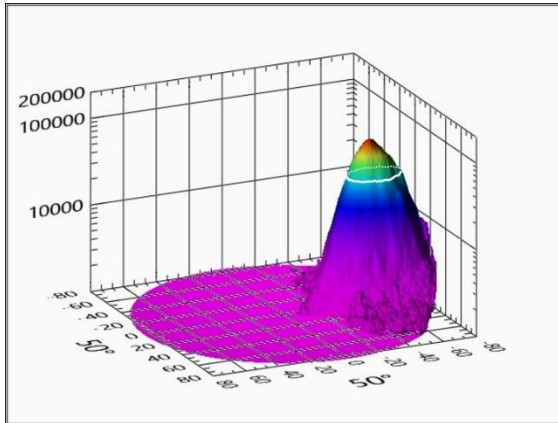

Figure 12: Typical BRDF measurement of a glare-reduced PV module (Figure 15) at an incidence angle of α =50°. The white line indicates the contour line for 30'000 cd/m^2.

The measured contour line is shown in Figure 13. An ellipse with a major and a minor axis is placed on top. This shows that the reflection surface that reflects with at least a certain luminance can be represented as an ellipse.
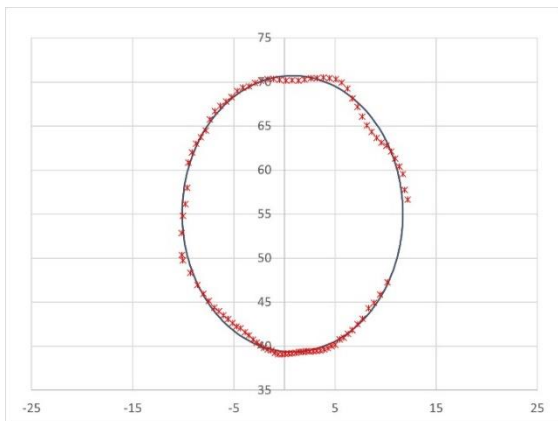

Figure 13: Elliptical approximation of the contour line at 30'000 cd/m^2 based on the example in Figure 12.

For each α in 10° steps, the luminance of the reflection is determined using the BRDF. The corresponding measurement results are shown in the form of elliptical contour lines in Figure 14. It can be seen that the ellipses hardly change for steep angles α. However, when α is flat, the reflecting surfaces become larger. For α starting from 50°, in accordance with Figure 3 in Chapter 2, the 30'000 cd/m^2 contour line is no longer specified, but instead the higher limit values.
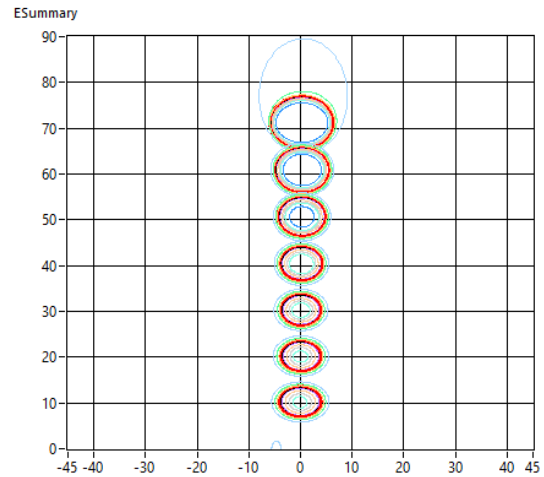

Figure 14: BRDF measurements shown as contour lines for different incident angles. Each set of circles refers to one specific incident angle with different colours for different luminance levels. The red circles show the contour line for a luminance of 30'000 cd/m^2.

For technical reasons the instrument that is used to measure the BSDF functions is not made for α of 80° or more. The measurements are therefore restricted to a maximum of $\alpha = 70°$. Even these measurements show, that or many glasses with only slight textures surfaces the 30'000 cd/m^2 contour line is passing over the 90° reflection angle.
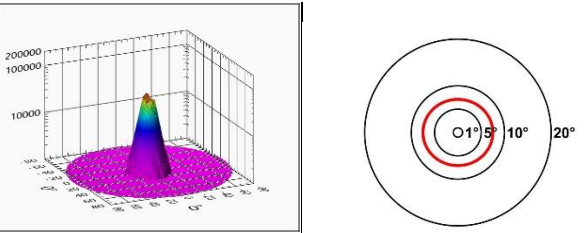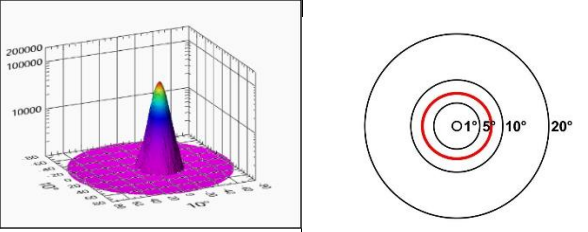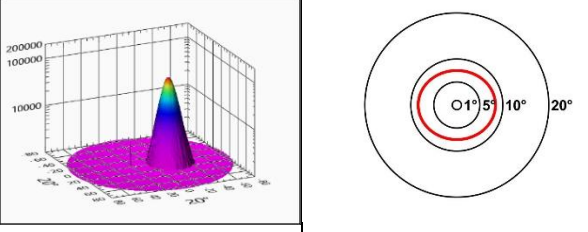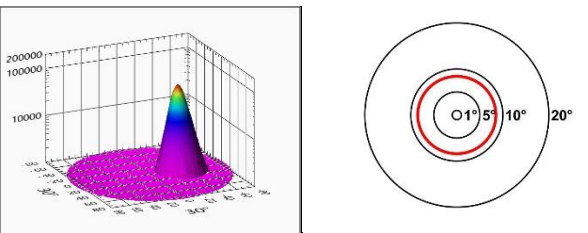
Assuming a luminance of 30'000 cd/m^2 being critical for glare hazards, a contour line at 30'000 cd/m^2 can be formed (see chapter 2 of this paper). Adopting the approach that was developed in Chapter 2, just means that the contour line is adjusted for higher angles α.
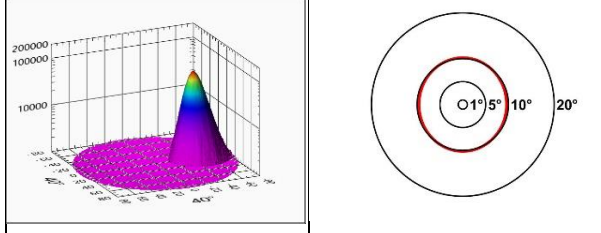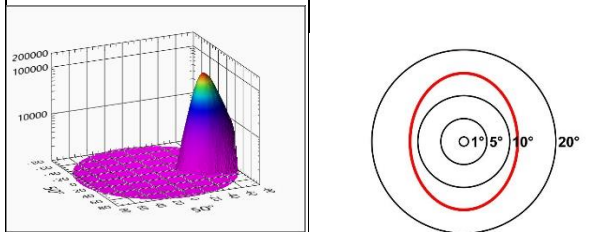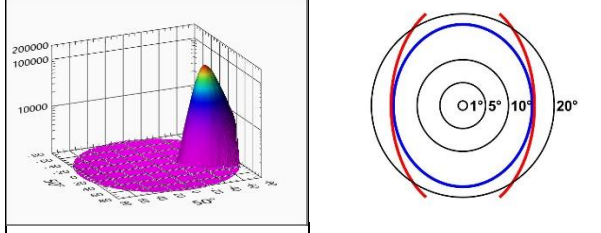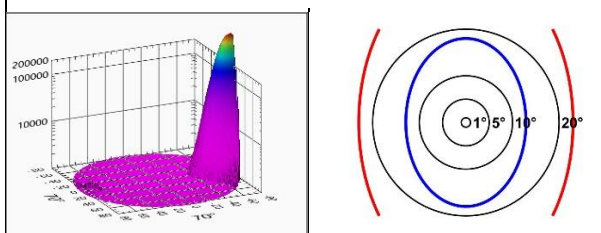
In analogy to Table I, all measurement results for α between 0° and 70° are shown in Table II. Because the measured solar glass differs from that in Chapter 3.2, the results are not directly comparable. However, both tables show that the approach can be presented in the same way regardless of the implementation and regardless of the product being measured.

Figure 15: Glass sample used to demonstrate the BRDF approach.

Table II: Left: Typical BRDF measurements of a glare-reduced PV module at different α. The z-axis for the luminance in cd/m^2 is logarithmic. The flat ground is caused by the lower cut at 1000 cd/m^2. Reflections below this value are irrelevant. Right: Luminance contour lines (approximated ellipses) for a typical PV surface. The red line indicates the contour line for 30'000 cd/m^2 and the blue line indicates the contour line when following the glare criteria defined in chapter 2.

Optical picture		Luminance image	
α (°)	Luminance max cd/m^2	Vertical axis (°)	Horizonal axis (°)
$\alpha = 0°$	22'000	7.1	7.5
Ellipse red: 30'000 cd/m^2			

$\alpha = 10°$	23'900	7.0	8.5
Ellipse red: 30'000 cd/m^2			

$\alpha = 20°$	26'400	7.5	8.4
Ellipse red: 30'000 cd/m^2			

$\alpha = 30°$	31'700	8.4	8.5
Ellipse red: 30'000 cd/m^2			

$\alpha = 40°$	43'400	10.2	9.6
Ellipse red: 30'000 cd/m^2			

$\alpha = 50°$	75'700	14.9	11.7
Ellipse red: 30'000 cd/m^2			

$\alpha = 60°$	182'500	23.3 (17.7)	15.7 (15.2)
Ellipse red: 30'000 cd/m^2 Ellipse blue: 40'000 cd/m^2			

$\alpha = 70°$	342'900	34.0 (18.0)	23.0 (12.9)
Ellipse red: 30'000 cd/m^2 Ellipse blue: 100'000 cd/m^2			

In comparison to Table I which is based on a standard PV module, the luminance of the glare-reduced PV module measured in Table II is much lower, but the beam spread is greater. Overall, this leads to a larger ellipse of possible glare. Luminance values for α between 0° to 20° are below 30'000 cd/m^2 and do therefore not cause glare according to Chapter 2.

Table III: Identified glare properties of standard module, based on luminance images of Chapter 3.2. Values in blue (in brackets) refer to the increased glare limit for angles of $a = 60°$ and larger.

α (°)	Limit (cd/m^2)	Lmax (cd/m^2)	Vertical Axis (°)	Horizontal Axis (°)
5°	30'000	594'000	5.0	5.7
10°	30'000	577'000	4.7	5.9
20°	30'000	539'000	4.9	5.4
30°	30'000	587'000	4.9	5.2
40°	30'000	495'000	5.1	5.0
50°	30'000	839'000	6.3	5.0
60°	40'000	2'400'000	7.4 (7.8)	4.7 (5.0)
70°	100'000	11'900'000	8.2 (9.8)	3.6 (4.4)
80°	400'000	47'500'000	8.2 (10.7)	2.3 (3.8)

Table IV: Identified glare properties of the glare-reduced module, based on BRDF approach of Chapter 3.3. Values in blue (in brackets) refer to the increased glare limit for angles of $a = 60°$ and larger.

α (°)	Limit (cd/m^2)	Lmax (cd/m^2)	Vertical Axis (°)	Horizontal Axis (°)
0°	30'000	22'300	7.1	7.5
10°	30'000	24'100	7.0	8.5
20°	30'000	26'700	7.5	8.4
30°	30'000	32'000	8.4	8.5
40°	30'000	44'000	10.2	9.6
50°	30'000	76'100	14.9	11.6
60°	40'000	185'000	17.7 (23.4)	15.2 (15.8)
70°	100'000	347'000	18.0 (34.0)	13.0 (23.0)
80°	400'000	na	na	na

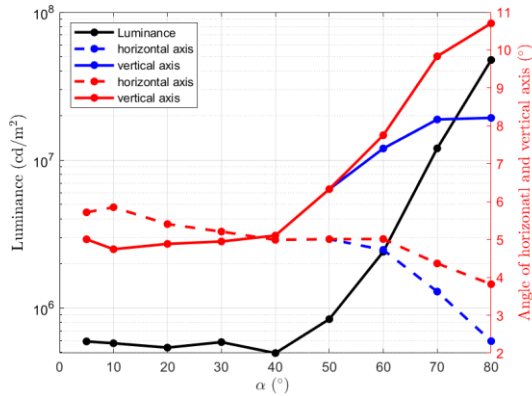**Figure 16:** Plotted glare properties of a standard module, based on luminance images (module presented in Chapter 3.2).
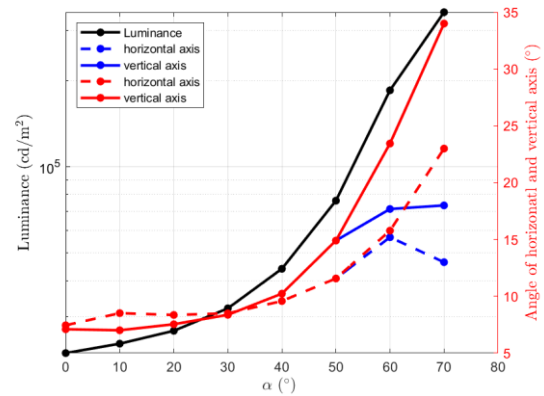

Figure 17: Plotted glare properties of a glare-reduced module, based on BRDF approach. Luminance values below the curve given in Figure 3 are not considered to cause glare (module presented in Chapter 3.3).

The angular dependence of the glares studied in Chapter 3.2 are summarised in Table III and Figure 16; the ones for Chapter 3.3. in Table IV and Figure 17, respectively. The results serve as an example of how the angular dependence of glare can be characterised in a simple two-dimensional graph.

The graphical representation (Figure 16 and Figure 17) allows to identify the glare characteristics of the studied modules and to compare them. Since the methods in Chapter 3.2. and 3.3. examine different PV modules, different glare characteristics can be seen. While the luminance for angles $\alpha < 50°$ is independent for the standard module investigated in chapter 3.2 (Figure 16), the luminance of the glare-reduced module investigated in chapter 3.3 (Figure 17) already increases for low α. Complementary behaviour is also seen in the horizontal axis of the glare ellipse. While the horizontal axis of glare ellipse of the standard module decreases with higher alpha, the same axis of the glare-reduced module rather increases with higher alpha.

6   PRESENTATION OF THE RESULTS AS A FUNCTION

The luminance as well as the horizontal and vertical axes can be represented as a function. Due to the various influences that lead to the characteristics of the two axes, empirical functions are sought. It seems clear that the best candidate can vary depending on the type of glass. It also makes a big difference whether the function should display the contour line with a constant 30'000 cd/m^2 or the one with higher limit values for flatter angles as introduced in Chapter 2. In this paper, the latter is chosen, as it has more relevance in practice.

Since the human eye sees logarithmically, it makes more sense to fit the logarithm of the luminance instead of the luminance itself. In this way, the fit for smaller luminance values deviates less from the measured values in absolute terms than for large luminance values, which is necessary to adequately represent the luminance for small alpha.

Two functions are tested to fit the logarithm of luminance. First, since the logarithm of the luminance (mostly) increases more with a larger angle of incidence α,

i.e. its second derivative is greater than or equal to 0, the following cosine function is tested:

$$ln(y) = a + \frac{b}{cos(\alpha)^c}$$

Here a, b, and c are parameters to be defined and α denotes the angle of incidence. Second, to better account for the fact that the luminance values can remain constant at low luminance values, α up to 50°, the biquadratic function, which has been investigated in [1] is tested:

$$ln'(y) = a \cdot \alpha^4 + b \cdot \alpha^2 + c$$

Table V: Parameters identified for the standard PV module measured in Chapter 3.2.

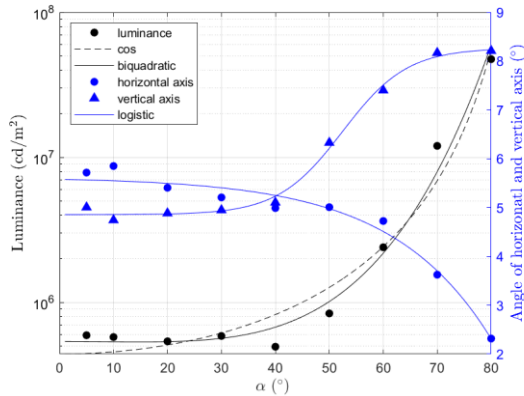|	Luminance		Vertical axis	Hor. axis
	cos	biquadratic	Logistic	
y	$e^{a+\frac{b}{cos(\alpha)^c}}$	$e^{a\cdot\alpha^4+b\cdot\alpha^2+c}$	$\frac{a}{1+e^{-(\alpha-b)\cdot d}}+c$	
a	2.173	$1.235\cdot 10^{-7}$	3.411	-1395
b	10.82	$-5.504\cdot 10^{-5}$	52.46	190.5
c	0.211	13.2	4.854	5.621
d	na	na	0.167	0.05465
R^2	0.958	0.983	0.99516	0.955

Figure 18: Fit of luminance image-based measurements of the standard PV module in Chapter 3.2.

The dimensions of the vertical and horizontal axes of the ellipse, on the other hand, are almost constant at steep angles of incidence, then increase and stagnate again at shallow angles α. For this reason, an S-curve (sigmoid function, logistic function) is chosen as the fit function.

$$y = \frac{a}{1+e^{-(\alpha-b)\cdot d}} + C$$

For the results in Table IV and Table III, the parameters in Table V and Table VI were found. The fits to the respective parameters are shown in Figure 18 and Figure 19

The biquadratic function seems to be more suitable for luminance values that remain constant during small incident angles (α <50°), which is the case for the standard solar glass of Chapter 3.2 (R2 = 0.983 vs. R2 = 0.958, see Figure 18). This may be because the biquadratic function,

unlike the cos function, is generally not a monotonically increasing function (between 0° and 90°).

The logarithm of the luminance values measured in Chapter 3.3. is monotonically increasing (see Figure 19) and can be fitted equally adequately by the biquadratic function (R2 = 0.993) as well as by the cos function (R2 = 0.993).

How well the logistic function agree with the measured axis values depends in particular on how the limit values for flat angles of incidence (α > 50°) are chosen. If these are greatly increased as suggested in this paper, sigmoid functions suitable. However, if the limit values were left at 30'000 cd/m², the biquadratic or cosine function would maybe be more suitable.

Table VI: Parameters identified for the glare-reduced PV module measured in Chapter 3.3.

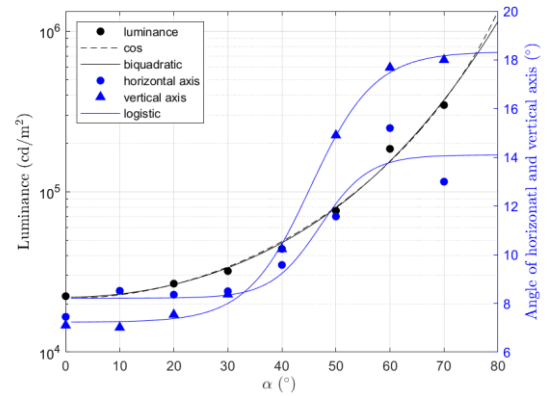|	Luminance		Vertical axis	Hor. axis
	cos	biquadratic	Logistic	
y	$e^{a+\frac{b}{cos(\alpha)^c}}$	$e^{a\cdot\alpha^4+b\cdot\alpha^2+c}$	$\frac{a}{1+e^{-(\alpha-b)\cdot d}}+c$	
a	18.5	$2.733\cdot 10^{-8}$	11.11	5.882
b	-8.52	$4.439\cdot 10^{-4}$	45.31	47.03
c	-0.3774	9.999	7.23	8.214
d	na	na	0.169	0.2229
R^2	0.992	0.993	0.998	0.918

Figure 19: Fit of BRDF approach-based measurements of the glare-reduced PV module in Chapter 3.3.

7 CONCLUSION

In this paper, a new definition and form of representation of the beam spreading of reflections from solar glasses was introduced and discussed. The proposal made is intended to describe properties regarding glare on PV modules in a simple and yet practically relevant way.

The proposal is based on the fact that glare on solar glasses is mostly elliptical and can therefore be characterised with a horizontal and vertical axis as well as the maximum luminance of the glare surface.

The method presented here works for glasses whose glare is elliptical. However, it does not work for characterising a reflection in general, especially when a PV module is produced with a glare-free glass. The method is particularly designed for implementation in software tools that are intended to calculate the possible glare on an optically slightly scattering surface in a simple way.

Although this paper examines various aspects of the form of glare, not all questions have been answered. Chapter 8 therefore lists which points should be further investigated.

8   OUTLOOK

The method presented here has not yet been used in a glare calculation tool and thus has not yet been tested for its practicality. This is proposed as the next step. Also, no product screening has been done yet. It is proposed to create a database of typical solar glasses and to record their luminance, as well as horizontal and vertical axis of the glare ellipse.

Furthermore, the paper has some inconsistencies that should be further investigated in the future:

1. It is assumed that the specular reflection for standard solar glasses is independent of the glass orientation. Figure 11 shows that this is not true or only partially true. To what extent this renders the statements of the paper invalid needs to be checked.
2. The validity restriction of the method presented in this paper refers to reflections that have an elliptical appearance. This restriction needs to be defined more precisely.
3. The methods in chapter 3.2 and chapter 3.3 should lead to identical results. The extent of the differences between the methods still needs to be validated.
4. The angle of incidence-dependent threshold value of 30,000 cd/m^2 to 400,000 cd/m^2 is proclaimed in this paper, but has not yet been confirmed. Further work and plausibility checks are necessary.
5. The geometric model in Chapter 3.1 does not fully correspond to reality and should be improved if this approach is to be pursued further.
6. The fit functions suggested in Chapter 6 should be tested, optimized and validated using different PV modules or surfaces.

9   ACKNOWLEDGEMENT

10   REFERENCES

[1]   Bucher, Christof; Danaci, Sirin; Wandel, Jasmin (25 Oktober 2021). Glare Hazard Analysis of Novel BIPV Module Technologies In: Solar World Congress. Monaco (virtual). 25.-29. Oktober 2021.

[2]   Andreas Bohren, 2015. Blendung von Solaranlagen Übersicht zur aktuellen Rechtslage. 25. OTTI Symposium Thermische Solarenergie, 6.-8. Mai 2015, Kloster Banz, Bad Staffelstein.

[3]   Clifford K. Ho, 2011, Methodology to Assess Potential Glint and Glare Hazards From Concentrating Solar Power Plants: Analytical Models and Experimental Validation, Journal of Solar Energy Engineering, Concentrating Solar Technologies Department, Sandia National Laboratories, Albuquerque, USA.

[4]   Clifford K. Ho, 2015, Solar Glare Hazard Analysis Tool (SGHAT) Technical Reference Manual, Sandia National Laboratories, Albuquerque, USA.

[5]   Florian Ruesch et al., 2015, Quantification of Glare from Reflected Sunlight of Solar Installations, SPF Institute for solar technology, HSR Rapperswil university of applied science, SHC 2015, International Conference on Solar Heating and Cooling for Buildings and Industry.

[6]   Florian Ruesch et al., 2016, Methode zur Quantifizierung der Blendung durch Solaranlagen - Vergleich mit anderen Materialien der Gebäudehülle, Institut für Solartechnik SPF, Hochschule für Technik Rapperswil HSR, 26. Symposium Thermische Solarenergie, 20.-22.04.2016 in Bad Staffelstein, Germany.

[7]   Referenz: Christof Bucher, Reflexionen an Photovoltaikanlagen, Ursachen und Lösungen, Bulletin electrosuisse, September 2021 [https://www.bulletin.ch/de/news-detail/reflexionen-an-photovoltaikanlagen.html].

[8]   Kanton Bern / Meteotest, Blendtool V1.2.0, www.blendtool.ch, Switzerland, accessed 11th of September 2023.

[9]   Photovoltaic Systems: Lower Levels of Glare and Reflectance vs. Surrounding Environment, Sunpower Corporation, Document # s107905 Rev A, 1st of October 2019

[10]   Data sheet, Kioto Solar, Sonnenkraft, Glas-Folien Solarmodul, Power-66 HC, 405Wp / 410Wp HC, 400Wp HC black, Blendreduziertes DEFLECT Glas, June 2022

[11]   EN 12665, Light and lighting - Basic terms and criteria for specifying lighting requirements, 2018

[12]   Marc Wittlich, 2010, Blendung – Theoretischer Hintergrund, Institut für Arbeitsschutz der Deutschen, Gesetzlichen Unfallversicherung (IFA), Sankt Augustin, Germany, May 2010

[13]   EN 12464-1, Light and lighting - Lighting of work places - Part 1: Indoor work places

[14]   Leonie Geerdinck: Glare perception in terms of acceptance and comfort. Graduation Report an: Faculty Industrial Engineering & Innovation Sciences, Technische Universiteit Eindhoven. http://alexandria.tue.nl/extra2/afstversl/tm/Geerdinck_2012.pdf, August 2012

[15]   Robert D Clear, Discomfort glare: What do we actually know? In: Lighting Research and Technology. vol. 45 no. 2 141-158 doi:10.1177/1477153512444527, April 2013

[16]   Hiroshi TAKAHASHI, Yoshinori KOBAYASHI, Shou ONDA, Takashi IRIKURA: Position Index for the Matrix Light Source. In: Journal of Light & Visual Environment. Vol. 31 (2007) No. 3 S. 128–133., https://www.jstage.jst.go.jp/article/jlve/31/3/31_3_128/_article

[17]   Julius Yellowhair and Clifford K. Ho, Assessment of Photovoltaic Surface Texturing on Transmittance Effects and Glint/Glare Impacts, Proceedings of the ASME 2015 Power and Energy Conversion.